Progress In Electromagnetics Research, Vol. 146, 133–142, 2014

An Efficient ISAR Imaging Method for Multiple Targets

Joo-Ho Jung[1], Kyung-Tae Kim[1], Si-Ho Kim[2], and Sang-Hong Park[3, *]

Abstract—This paper proposes an efficient method to obtain ISAR images of multiple targets flying in formation. The proposed method improves the coarse alignment and segmentation of the existing method. The improved coarse alignment method models the flight trajectory using a combination of a polynomial and Gaussian basis functions, and the optimum parameter of the trajectory is found using particle swarm optimization. In the improved segmentation, the binary image of the bulk ISAR image that contains all targets is constructed using a two-dimensional constant false alarm detector, then the image closing method is applied to the binary image. Finally, the connected set of binary pixels is used to segment each target from the bulk image. Simulations using three targets composed of point scattering centers and the measured data of the Boeing747 aircraft prove the effectiveness of the proposed method to segment three targets flying in formation.

1. INTRODUCTION

Inverse Synthetic Aperture Radar (ISAR) imaging is a technique to generate a two-dimensional high resolution image of a target [1–4]. Among many ISAR imaging techniques, range-Doppler imaging (RDI) is widely used because of its simplicity [5]. However, when multiple targets occur in a single radar beam, imaging each target separately can be difficult. Algorithms have been proposed to solve this problem, but none is fully satisfactory. One method assumes that the number of targets is known [6] and another requires that the range migrations of all targets be equal [7]. Other conventional methods also have limitations [8, 9].

Recently, we proposed an efficient ISAR segmentation method that is composed of three steps; coarse range alignment, image segmentation and enhancement of the segmented images [10]. The key steps of this method are the coarse range alignment in which every single pixel has the same weight on the cost function and the segmentation of ISAR images coarsely formed after phase adjustment. However, the existing coarse alignment and segmentation methods have some problems. In the coarse alignment, the range-Doppler image can be seriously blurred if one of the several segments is poorly aligned. In the segmentation, if targets are narrowly spaced, two targets may be partially accommodated in a window simultaneously.

In this paper, we propose an improved version of the coarse alignment and the segmentation methods recently proposed in [10]. The proposed coarse alignment models the total trajectory using a combination of a polynomial and Gaussian basis functions. The initial values for the parameters of the polynomial and the Gaussian basis functions are determined by fitting the model to the center of mass (COM) curve of the range profile history using a least square curve-fitting algorithm, which utilizes the gradient descent rule. Then the parameters are optimized using particle swarm optimization (PSO) [11]. In the image segmentation, the image closing method in morphological image processing (MIP) [12] is utilized. Image closing consists of image dilation followed by image erosion using a structuring element.

Received 29 April 2014, Accepted 11 May 2014, Scheduled 16 May 2014

* Corresponding author: Sang-Hong Park (radar@pknu.ac.kr).

[1] Department of Electrical Engineering, Pohang University of Science and Technology, Pohang, Gyungbuk, Korea. [2] Agency for Defense Development, Daejeon, Korea. [3] Department of Electronic Engineering, Pukyong National University, Busan, Korea.

In this method, a binary image of the bulk image is constructed using a 2D constant false alarm (CFAR) detector [13]. Image closing is then applied to the binary image. The connected set of pixels in the closed image is used to segment each target from the bulk image. In simulations using point scatterer models of two Su-35s and one F-14, and the measured data of the real Boeing747, the proposed method is more accurate and requires less computation in coarse alignment and successfully segments the bulk image into sub-images.

2. SUMMARY OF THE SEGMENTATION ALGORITHM

The segmentation algorithm proposed in [10] is composed of three steps, (1) an initial RDI of the whole set of targets to obtain a bulk image; (2) separation of the bulk image into component images using an appropriate segmentation algorithm, and (3) a second RDI, in which each ISAR image is enhanced using range alignment and phase adjustment (Fig. 1).

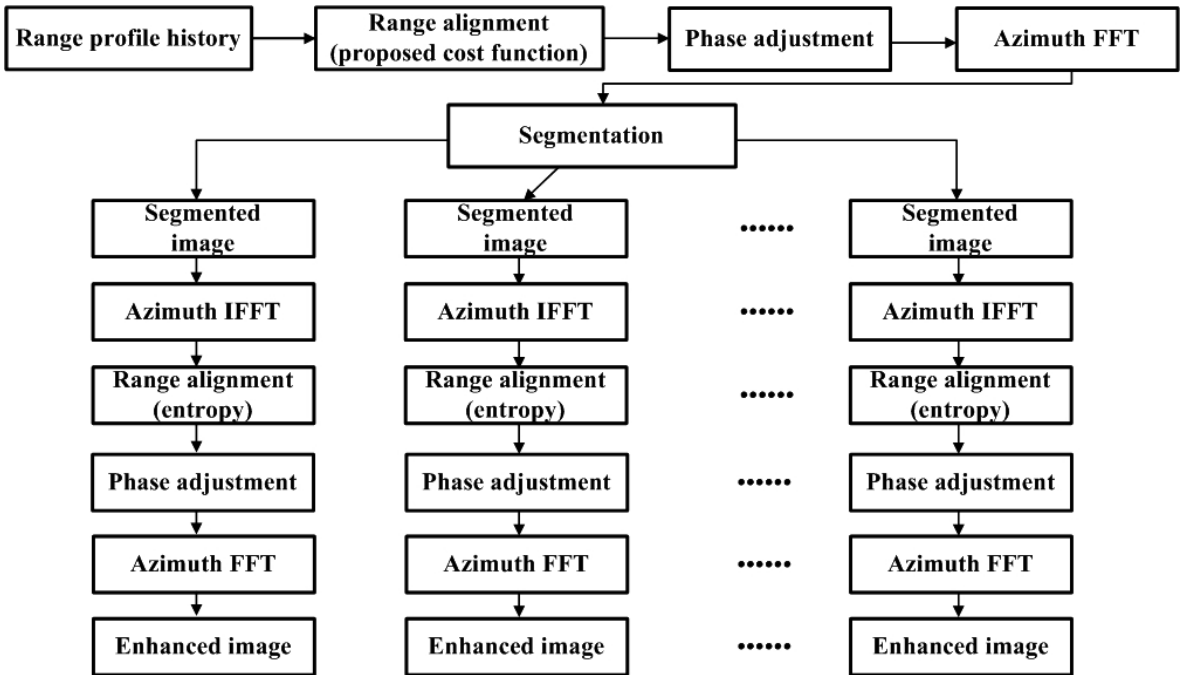

Figure 1. Segmentation method proposed in [10].

In the first step, a general range-Doppler algorithm is applied to coarsely separate targets in the 2D range-Doppler domain. A new range alignment method which aligns range profiles using a polynomial that best represents the trajectory was proposed. Particle-swarm optimization (PSO) was used to estimate the parameters of the polynomial by using the number of pixels lying on the trajectory as a cost function. A segmented alignment algorithm was also introduced to align range profiles if the polynomial did not fit the flight trajectory.

The second step is the segmentation of the ISAR image of each target separately positioned in the 2D range-Doppler domain. In this step, a simple method was utilized, which groups pixels belonging to a target which can be accommodated in a window of the target size. In this process, a binary image using the average pixel power as a threshold was constructed and COM using the pixels with the window was calculated in each iteration until the number of the pixels within the window stopped increasing. The third step is the enhancement of each image. Range alignment and phase adjustment were repeated after converting each segmented range-Doppler image into a range-time domain using inverse fast Fourier transforming in each range bin. Then fast Fourier transforming (FFT) was performed in each range bin to derive the ISAR image of each target.

3. PROPOSED METHOD

3.1. Improved Coarse Alignment

The main problem of the segmented alignment in the coarse alignment is that the required computation is large because the cost function must be optimized for each segment. If the number of segment is reduced to save computation time, mismatch between the polynomial and the trajectory may occur and this causes serious blurring of the bulk image (Fig. 2). In Fig. 2, three segments were used for the alignment and each segment was poorly aligned due to the mismatch between the polynomial and each segment (Fig. 2(a)). As a result, the ISAR image became blurred (Fig. 2(b)).

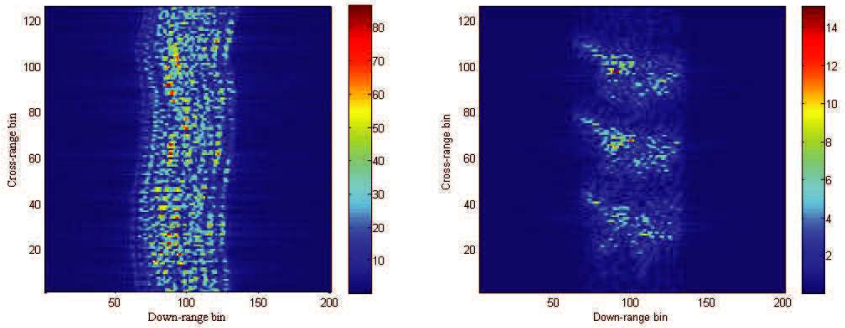

(a) Alignment result (b) ISAR image of (a)

Figure 2. Segmented alignment result (3 segment); range profiles are poorly aligned and ISAR is blurred because of the small number of segments.

In this paper, we model the target trajectory by using a combination of a polynomial and Gaussian basis functions and applying the estimation procedure as given in [14]. Given M range profiles each having N range bins, the function that represents the target trajectory is expressed as

$$f(x) = \sum_{i=0}^{L} p_i x^i + \sum_{i=0}^{G} a_i \exp\left(-\left(\frac{x-b_i}{c_i}\right)^2\right), \tag{1}$$

where $f(x)$ is the trajectory function; $x = 0 - M - 1$ in increments of 1; p_i are parameters for the polynomial; a_i, b_i, c_i are parameters for the Gaussian basis functions; L is the order of the polynomial; $G+1$ is the number of Gaussian functions. This method polynomial was applied to range alignment of a single target using the maximum energy [14] and was less accurate than the nonparametric method [15]. However, a combination of this polynomial and the cost function defined in [10] effectively aligns RPs of multiple targets and generates the bulk image.

For the estimation of the parameters in (1), we apply the gradient-based method in [14]. In setting the initial values of the parameters in (1), we use the parameters that fit (1) to the COM curve of the range profile history. The COM_m of the mth range profile is defined as

$$\mathrm{COM}_m = \sum_{n=0}^{N-1} \frac{|G_m(n)| \times n}{\sum_{k=0}^{N-1} |G_m(k)|}, \tag{2}$$

where G_m is mth range profile, and N is the same as in (1). The COM curve can approximate the trajectory because COMs are located in the target region. The COM curve can be downsampled to a smaller number of points to better fit the trajectory function. Assuming the vector $\bar{s}$ represents the parameters in (1), we use the gradient-based least square solution that minimizes the error between the COM curve and the estimated function $f(x, \bar{s})$, as follows:

$$E = \sum_{i=1}^{M} e_i^2, \quad e_i = \mathrm{COM}_i - f(x_i, \bar{s}), \tag{3}$$

where x_i is the ith element of x in (1), i.e., the index of the range profile i that is used for COM_i. The jth element s_j of $\bar{s}$ that minimizes E is obtained by finding the zero gradient, which is

$$\frac{\partial E}{\partial s_j} = 2\sum_{i=1}^{M} e_i \frac{\partial e_i}{\partial s_j} = 0. \tag{4}$$

Because of the non-analytic nature $\bar{s}$, $\bar{s}$ is obtained iteratively until (4) converges. The update formula for the iteration $k+1$ by is

$$\bar{s}^{k+1} = \bar{s}^k + \Delta\bar{s}. \tag{5}$$

$\Delta\bar{s}$ is obtained by applying the Newton algorithm [16] as follows:

$$\left(J_s^T J_e\right)\Delta\bar{s} = -J_e^T\bar{e}, \tag{6}$$

where $\bar{e}$ is the vector composed of e_is and J_e is the Jacobian matrix with respect to $\bar{e}$.

Once the initial values are found using the gradient-based method, the parameters s can be optimized using a global optimization algorithm and the cost function defined in [10]. We use PSO because it is easy to implement and has been proven to be efficient for several engineering problems [16]. The particle dynamics which update each particle is as follows:

$$\bar{\mathrm{v}}_i(t) = \phi\bar{\mathrm{v}}_i(t-1) + \rho_1(\bar{\mathrm{s}}_{pbest} - \bar{\mathrm{s}}_i(t)) + \rho_2(\bar{\mathrm{s}}_{gbest} - \bar{\mathrm{s}}_i(t)), \tag{7}$$

where t is the generation number, ϕ is the inertial weight, $\rho_1 = r_1c_1$, $\rho_2 = r_2c_2$. $\bar{\mathrm{s}}_{pbest}$ and $\bar{\mathrm{s}}_{gbest}$ are the particle best and the global best respectively. Values of c_1, c_2 are both > 1, subject to the constraint $c_1 + c_2 < 4$; r_i are drawn from a random uniform distribution from 0 to 1. The position of the particle i in generation $t+1$ calculated as follows:

$$\bar{\mathrm{s}}_i(t+1) = \bar{\mathrm{v}}_i(t) + \bar{\mathrm{s}}_i(t). \tag{8}$$

For $t = 1$, several random vectors were set with elements of the uniform probability distribution between $s \pm \gamma s$, where $\gamma < 1$ is a constant.

3.2. Improved Segmentation

In [10], we assumed that the window size of the target is known. However, this assumption is weak because the exact target size of the target is probably not known. Lack of knowledge of target size can result in poor segmentation because one target cannot be fully accommodated in a window if the window is too small, and two or more targets can be accommodated if the window is too large. Poor segmentation can occur when the target is heading directly at the radar, because the elevation angle variation contributes to the angular variation more than does the azimuth variation. In this case, the image of the target is compressed in the range-Doppler domain and the whole set of targets may be accommodated in one window (Fig. 3).

The segmentation method proposed in this paper is unaffected by window size. This method is based on MIP [12]. In the first preprocessing step, to remove the clutter-like effect caused by the interference among multiple aircraft, we convert the bulk image to a binary image using the conventional CFAR detector as follows [13]:

$$T(x) = \frac{x - \hat{\mu}_c}{\hat{\sigma}_c}, \tag{9}$$

where x is the amplitude of the test pixel, $\hat{\mu}_c$ the estimated mean of the clutter amplitude, and $\hat{\sigma}_c$ the estimated standard deviation of the clutter amplitude. $\hat{\mu}_c$ and $\hat{\sigma}_c$ are calculated from the pixels that surround the total image. If $T(x)$ is larger than a threshold, the corresponding binary pixel value is 1; it is 0 otherwise. Because air-to-air or land-to-air ISAR images do not suffer seriously from clutter, the CFAR detector successfully removes the clutter effect efficiently.

The second step is image closing using MIP. Imaging closing smoothes sections of contours, generally fuses narrow breaks and long thin gulfs, and eliminates small holes. Because ISAR images may contain numerous small holes due to the finite number of scatterers, the CFAR-detected binary image also contains numerous small holes. Image closing fills these small holes efficiently. Image closing is defined as image dilation followed by image erosion:

$$C(A, B) = (A \bullet B) \circ B, \tag{10}$$

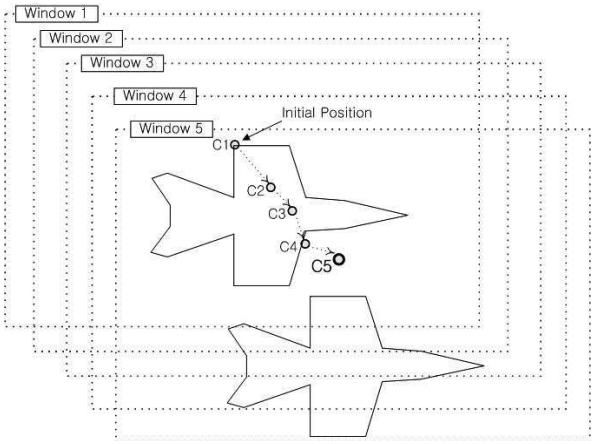

Figure 3. Image segmentation using a window larger than twice the target size [10]; Cn = center of mass of window n. Sums of converted pixel values within windows are compared sequentially until the sum stops increasing. However, each image may not be segmented properly because of the large window size.

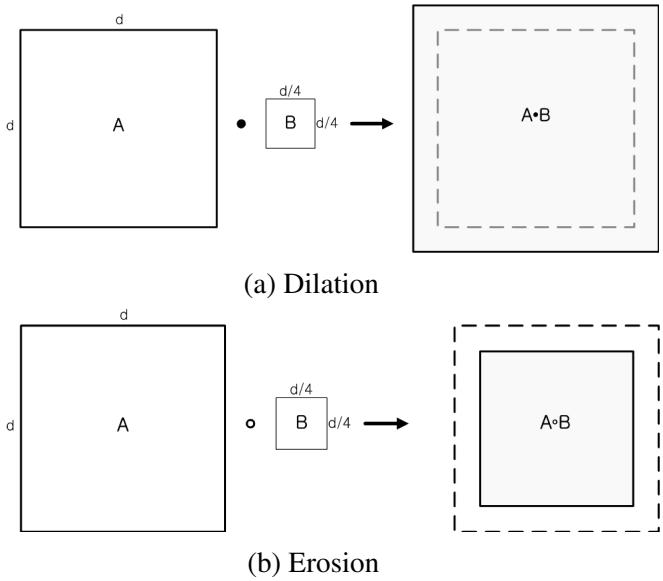

Figure 4. Image dilation and erosion.

where C is the closing operation, $\bullet$ the dilation operation, and $\circ$ the erosion operation. Assuming that an image A and the structuring element B are in Z^2 space, the dilation of A by B is defined as follows (Fig. 4(a)) [12]:

$$(A \bullet B) = \left\{ z | \left(\hat{B} \right)_z \cap A \neq \emptyset \right\}, \tag{11}$$

where $\hat{B}$ is the reflection of set B defined as

$$\hat{B} = \{ w | w = -b, \text{ for} \in B \}, \tag{12}$$

and $(A)_z$ is the image translation by point $z = (z_1, z_2)$ defined by

$$(A)_z = \{ c | c = a + z, \text{ for } a \in A \}. \tag{13}$$

In a similar manner, the image erosion of A by B is as follows (Fig. 4(b)) [12]:

$$A \circ B = \{ z | (B)_z \subseteq A \}. \tag{14}$$

The third step is searching for the connected set formed by the image closing. Because some pixels can be falsely detected by the CFAR detector, we decide in this step whether the connected set belongs to a target using the number of pixels in the connected set. If the number is very small, the connected set is discarded; if not, it is used for the segmentation of the target from the image.

In the simulation, we used the same motion and radar parameters as in [10]. Two Su-35 and one F-14 fighters composed of isotropic scattering centers were used. We assumed that the three aircraft flew in the $[-1 \ -1 \ 0]$ direction with velocity $v = 300\,\mathrm{m/s}$ and acceleration $a = 10\,\mathrm{m/s^2}$ starting from the initial positions $[x_1 \ y_1 \ z_1] = [0.310 \ 50.0 \ 3.0]\,\mathrm{km}$ (first Su-35), $[x_2 \ y_2 \ z_2] = [0.335 \ 50.0 \ 3.0]\,\mathrm{km}$ (second Su-35), $[x_3 \ y_3 \ z_3] = [0.285 \ 50.0 \ 3.0]\,\mathrm{km}$ (F-14). The simulation used pulse repetition frequency $= 2$ kHz, center frequency $f_0 = 9.15\,\mathrm{GHz}$, $B = 200\,\mathrm{MHz}$ (0.75 m range resolution), and sampling rate $= 512\,\mathrm{MHz}$. Pulses were transmitted for 4.40 s (9800 pulses) to obtain cross-range resolution similar to the down-range resolution and the collected pulses were down-sampled to 128 equally spaced pulses. The signal-to-noise ratio (SNR) used was assumed to be 10 dB, and η to calculate the cost function was set to 5%. The window size used for the segmentation was 100×40 which is much larger than a single target.

4. SIMULATION RESULTS

The gradient-based curve-fitting method fits the COM curve well (Fig. 5). The COM curve was downsampled to 64 points to better fit the trajectory function and with $L = 2$ and $G = 6$ (seven Gaussian basis functions) in (1); iteration was stopped when the average of the absolute difference between the function and the COM curve was < 1.5. Then, with γ set to 0.1, PSO was used to optimize the parameters of the function.

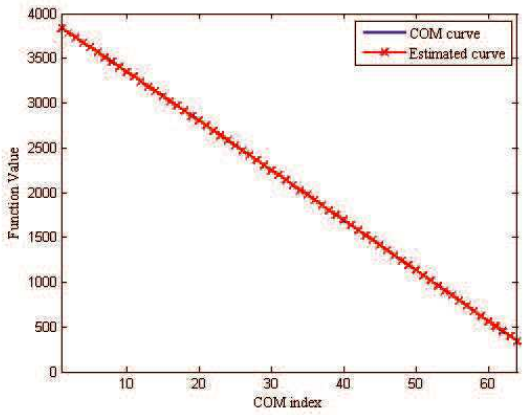

Figure 5. COM curve and estimated curve.

The alignment result (Fig. 6(a)) is much better than that of the segmented alignment with three segments (Fig. 2(b)). As a result, the focus of the ISAR image after phase adjustment is improved and scatterers of each target are well distributed in the 2D range-Doppler domain (Fig. 6(b)). Therefore, each target can be segmented and further enhanced using the method in [10]. This result proves that the proposed trajectory function describes the flight trajectory well. Running the program written in Matlab R2007a in Windows XP on an Intel Quadcore processor, the computation time for the proposed alignment was 1.9723 s which is much less than the 6.7712 s required using segmented alignment.

Because the 100×40 window was much larger than a single target, the segmented image from Fig. 6(b) contains parts of two targets from the bulk image (Fig. 7). The existing CFAR detector successfully detects the image pixels (Fig. 8(a)). To determine the threshold, various simulations were conducted and values between 2 and 4 yielded the good results. In this paper, we used 3 ($= 3\hat{\sigma}_c$) as a threshold. The detected pixels constitute narrow breaks and small holes. We used a flat disk-shaped structuring element (Fig. 8(b)) in closing the image. After the image closing operation, the images are

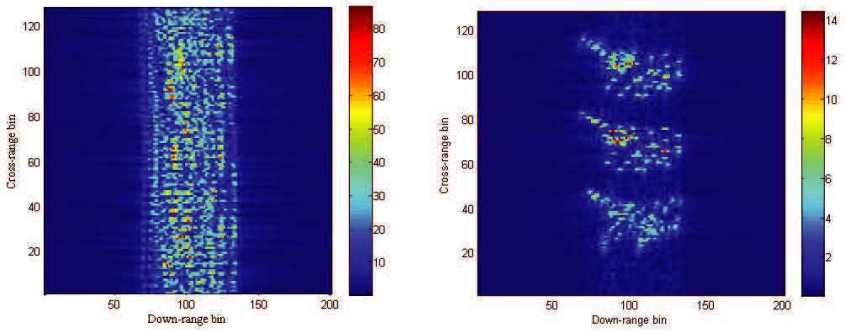

(a) Coarse alignment result (b) ISAR image of (a)

Figure 6. Alignment result using proposed method; range profiles are well aligned and ISAR is focused because of the trajectory function matches the trajectory.

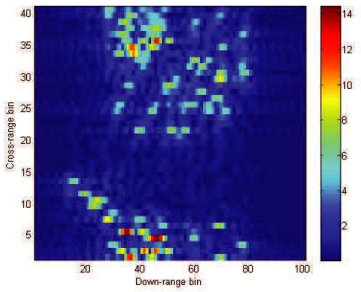

Figure 7. Segmentation result using the 100 40 window; two targets are partially accommodated in the segmented image.

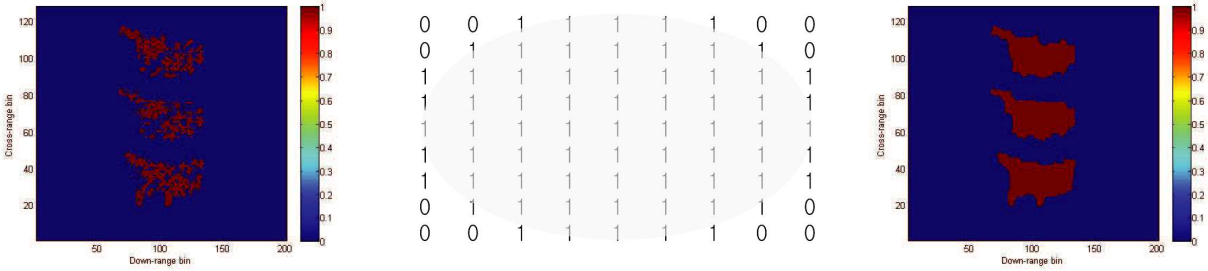

(a) CFAR detected image of Fig. 4(a) (b) Disk-shaped structuring element (c) Closed image of (a)

Figure 8. CFAR detection and image closing result.

well-closed (Fig. 8(c)). Other structuring elements such as a rectangle and a diamond yielded similar results. Finally, three targets in the bulk image were successfully segmented and ready for the further enhancement proposed in [10] (Figs. 9(a)–(c)).

To demonstrate the efficiency of the proposed method, the IASR image of a real Boeing747 was measured by using an X-band radar with $B = 100\,\text{MHz}$ (1.5 m resolution) and segmentation of the ISAR images of the three Boeing747s flying in formation was conducted. For this purpose, the range profiles of the Boeing747 obtained at two different time frames (0.2–0.6 and 1.1–1.5 s) were superposed; to simulate three aircraft flying in formation, the range profiles measured for 0.2–0.6 s were used twice with the second set of range profiles shifted in cross-range direction. To remove the image blurring caused by the effect of jet engine modulation, the method based on the adaptive chirplet representation was applied [17]. Then, to demonstrate the effectiveness of the proposed coarse alignment method, the

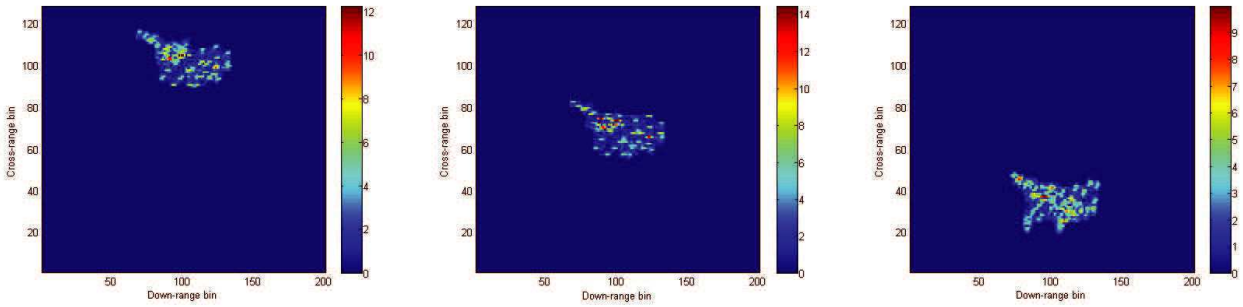

(a) Target 1 (b) Target 2 (c) Target 3

Figure 9. Segmentation result using the proposed method.

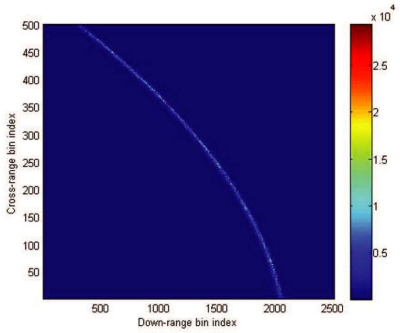

Figure 10. Range profile history of three Boeing747s flying in formation.

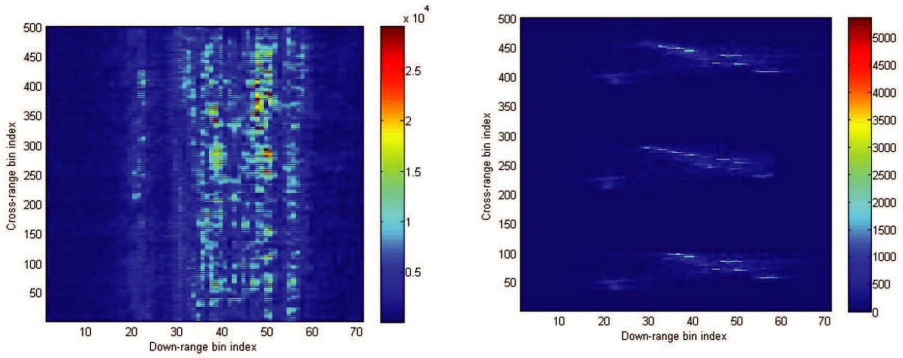

(a) Coarse alignment result (b) ISAR image of (a)

Figure 11. Alignment result using proposed method (measured data of Boeing747); range profiles are well aligned and ISAR is focused by the proposed method.

superposed range profiles were shifted by using the following polynomial (Fig. 10):

$$s(x) = -0.002x^2 - 5x + 2500, \tag{15}$$

where x is the range profile index. Because $s(x)$ is real-valued, a range profile x was shifted by the nearest integer of $s(x)$.

Range profiles are well-aligned by the proposed method because the proposed polynomial exactly matched $s(x)$ (Fig. 11(a)). As a result, the three Boeing747s are properly shown in the bulk ISAR image obtained after range alignment and phase adjustment (Fig. 11(b)). The three ISAR images segmented by the proposed method and enhanced by range alignment and phase adjustment clearly represent each target, proving the effectiveness of the proposed method (Figs. 12(a)–(c)).

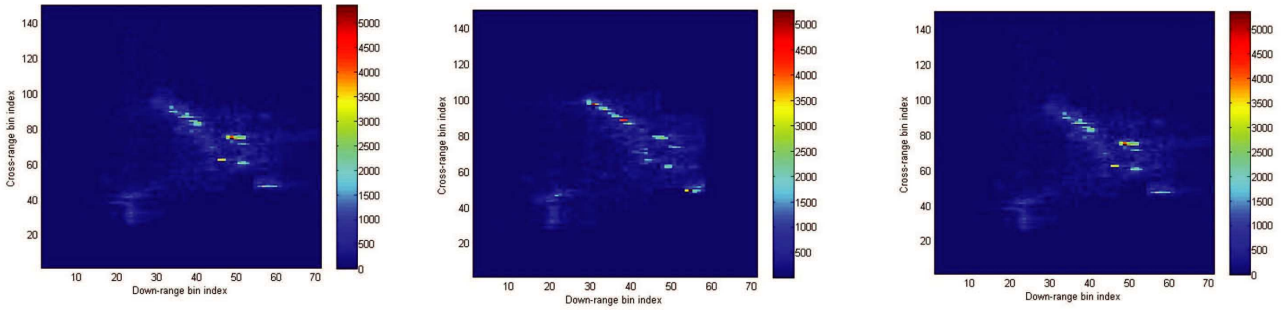

(a) Target 1 (b) Target 2 (c) Target 3

Figure 12. Segmentation result using the proposed method (measured data of Boeing747); Boeing747 is well represented by the segmented image.

5. CONCLUSION

In this paper, we propose an improved coarse alignment and segmentation method to segment images in the 2D range-Doppler domain of multiple targets flying in formation. In range alignment, the proposed method models the flight trajectory using a combination of a polynomial and Gaussian basis functions. Using the gradient-based Gauss-Newton algorithm, initial values of the parameters are found by fitting the trajectory function to COM curve. Then, PSO is applied to optimize the trajectory function. In segmentation, the proposed method utilizes the image closing method in the MIP. A binary image of the bulk image is constructed using 2D CFAR detector. Then image closing is applied to the binary image. The connected set of the closed image is used to segment each target from the bulk image. In simulations using the point scatter models of two Su-35s and one F-14, and the measured data of the real Boeing747, the calculated trajectory represents the true flight trajectory well and provides well-aligned range profiles and well-focused ISAR images. The proposed segmentation method successfully segments the bulk image into sub-images, whereas the existing method cannot do so when the window size is much larger than the target.

ACKNOWLEDGMENT

This work was supported by the STRL (Sensor Target Recognition Laboratory) program of Defense Acquisition Program Administration and Agency for Defense Development.

REFERENCES

1. Chen, C. C. and H. C. Andrews, "Target-motion-induced radar imaging," *IEEE Trans. Aerosp. Electron. Syst.*, Vol. 16, No. 1, 2–14, Jan. 1980.
2. Park, S.-H., J.-H. Lee, and K.-T. Kim, "Performance analysis of the scenario-based construction method for real target ISAR recognition," *Progress In Electromagnetics Research*, Vol. 129, 137–151, 2012.
3. Park, J.-H. and N. H. Myung, "Enhanced and efficient ISAR image focusing using the discrete Gabor representation in an oversampling scheme," *Progress In Electromagnetics Research*, Vol. 138, 227–244, 2013.
4. Naqvi, A. and H. Ling, "Time-frequency and ISAR characteristics of wind turbines with higher order motions," *Progress In Electromagnetics Research*, Vol. 143, 331–347, 2013.
5. Ausherman, D. A., A. Kozma, J. L. Walker, H. M. Jones, and E. C. Poggio, "Development in radar imaging," *IEEE Trans. Aerosp. Electron. Syst.*, Vol. 20, No. 4, 363–400, Jul. 1984.
6. Wang, A., Y. Mao, and C. Chen, "Imaging of multi-targets with ISAR based on the time-frequency distribution," *Proc. IEEE Int. Conf. Acoust Speech Signal Processing,* Vol. 5, 173–176, 1986.

7. Wu, X. and Z. Zhu, "Simultaneous imaging of multiple targets in an inverse synthetic aperture radar," *Proc. IEEE 1990 National Aerospace and Electronics Conference,* Vol. 1, 210–214, May 1990.
8. Mao, Y., G. Chen, and J. Wang, "SAR/ISAR imaging of multiple moving targets based on combination of WVD and HT," *1996 CIE International Conference of Radar Proceedings,* 342–345, Oct. 8–10, 1996.
9. Kazuhiko, Y., I. Masafumi, F. Takahiko, and K. Tetsuo, "An ISAR imaging algorithm for multiple targets of different radial velocity," *Electronics and Communications in Japan (Part I: Communications),* Vol. 86, No. 7, 1–10, Mar. 2003.
10. Park, S.-H., H.-T. Kim, and K.-T. Kim, "Segmentation of ISAR images of targets moving in formation," *IEEE Trans. Geosci. Remote Sens.*, Vol. 48, No. 4, 2099–2108, Apr. 2010.
11. Kennedy, J. and R. C. Eberhart, *Swarm Intelligence*, Academic Press, 2001.
12. Gonzales, R. C. and R. E. Woods, *Digital Image Processing*, Prentice Hall, 2002.
13. Wang, J. and X. Liu, "Improved global range alignment for ISAR," *IEEE Trans. Aerosp. Electron. Syst.*, Vol. 43, No. 3, 1070–1075, Jul. 2007.
14. Park, S.-H., H.-T. Kim, and K.-T. Kim, "Enhanced range alignment using a combination of a polynomial and Gaussian basis functions," *Progress In Electromagnetics Research*, Vol. 95, 381–396, 2009.
15. Park, S.-H., "A study on range alignment for long-range ISAR imaging and segmentation of ISAR images for aircraft flying in formation," Ph.D. Dissertation, Department of Electrical Engineering, POSTECH, Pohang, Korea, 2010.
16. George, A., F. Seber, and C. J. Wild, *Nonlinear Regression*, Wiley-Interscience, 2003.
17. Jung, J.-H., K.-T. Kim, and S.-H. Park, "Removal of JEM signal by accurate estimation of initial parameters of chirplet basis functions," *Progress In Electromagnetics Research*, Vol. 141, 607–618, 2013.